Journal of Hydrology 613 (2022) 128391

Contents lists available at ScienceDirect

Journal of Hydrology

journal homepage: www.elsevier.com/locate/jhydrol

Research papers

Sediment transport investigation in a karst aquifer hypothesizes controls on internal versus external sediment origin and saturation impact on hysteresis

Leonie Bettel [a], Jimmy Fox [a,*], Admin Husic [b], Junfeng Zhu [c], Nabil Al Aamery [a], Tyler Mahoney [d], Ariel Gold-McCoy [a]

[a] Civil Engineering at the University of Kentucky, USA
[b] Civil, Environmental, and Architectural Engineering at the University of Kansas, USA
[c] Kentucky Geological Survey, USA
[d] Civil Engineering at the University of Louisville, USA

ARTICLE INFO

This manuscript was handled by Jiri Simunek, Editor-in-Chief, with the assistance of Yonghong Hao, Associate Editor

Keywords:
Sediment transport
Karst
Sediment sources
Hysteresis
Antecedent conditions
Sediment timing

ABSTRACT

Karst springs serve as major drinking water sources for the global population, yet there remains uncertainty regarding how contaminants like sediment are routed through karst. We find knowledge gaps pertaining to the processes that control the timing and magnitude of sediment delivery. To close these knowledge gaps, we: (1) collected high-frequency sediment and conductivity data from three surface streams and two cave sites in the inner bluegrass region of Kentucky, USA; (2) analyzed sediment hysteresis for 51 storm events over a two year period; (3) numerically modeled sediment transport through the aquifer; and (4) contextualized our results with a meta-analysis of ten karst springs in Europe and North America. Our results showed that 80% of storm events derived their sediment from external inputs through sinking streams while the remaining 20% were characterized by only internal resuspension of previously deposited cave sediment. We found that internal sediment transport was proportional to fluid shear stress in the cave and occurred exclusively during fully saturated aquifer conditions prior to the storm event. During partially-saturated aquifer conditions, externally sourced sediment pulses were efficiently routed to the spring irrespective of shear in the conduit network. Sediment hysteresis in surface streams was clockwise whereas the cave sites experienced counter-clockwise behavior. Clockwise and counter-clockwise hysteresis typically refer to proximal and distal sourcing for streams, but our findings suggest that this interpretation is not valid for subsurface karst settings. Hysteresis patterns for karst show dependence on the antecedent water conditions in the aquifer and internal versus external sourcing. meta-analysis results show that, despite high variability, counter-clockwise patterns of sediment hysteresis are very common for karst, which contrasts sediment hysteresis in surface streams. Results suggest that external sediment loading rather than internal resuspension is the most common control of sediment load at springs, which should inform management of karst groundwater resources.

1. Introduction

Twenty-five percent of the world's drinking water originates from karst aquifers (Leibundgut, 1998), which are particularly susceptible to contamination due to fast travel times in the subsurface (White, 2002). We find knowledge gaps regarding the sediment transport processes in karst, which limits our ability to accurately formulate predictive equations and understand the timing and source of sediment arriving at karst springs. Two decades ago, White (2002) reported sediment transport in karst as an open topic with many areas that still need to be investigated. Since that time, scientists advanced our understanding of sediment transport in karst aquifers and cave systems, with results such as: the occurrence of internal erosion of stored sediment in caves and externally-sourced sediment transport from sinking streams during storm events (Herman et al., 2008; Goldscheider et al., 2010); a suite of erosion, deposition and transport processes potentially occurring in karst caves (Herman et al., 2008; Reed et al., 2010); and the control of hydraulic conveyance limits on the sediment transport carrying capacity of the flow (Husic et al., 2017a,b). However, prediction methods and interpretation of hydrologic data remains understudied for sediment

* Corresponding author.
E-mail address: james.fox@uky.edu (J. Fox).

https://doi.org/10.1016/j.jhydrol.2022.128391
Received 13 April 2022; Received in revised form 15 July 2022; Accepted 18 August 2022
Available online 28 August 2022

transport in karst despite the potential detrimental impacts of sediment on drinking water.

Sediment transport in karst relies on both external and internal processes (Herman et al., 2008; Goldscheider et al., 2010). External sediment sources can be transported into the subsurface through surficial connections to the karst aquifer, which include sinkholes and sinking streams (White, 2002). The high permeability of karst aquifers defined by fracture networks and cave systems enables this external sediment to transport relatively quickly to karst springs. Sediment deposits can also occur in caves as the transport capacity of the fluid reduced due to the loss in flow energy from sinking streams entrance (Husic et al., 2017a). These sediment deposits become internal sediment that can be resuspended in subsequent hydrologic events (Dogwiler & Wicks, 2004; Reed et al., 2010). However, the distribution of hydrologic events causing transport of internal and external sediment and the processes controlling their transfer remains an advancement needed for prediction (Cheng et al., 2020; Nerantzaki et al., 2015).

Sediment hysteresis is a method to infer sediment sources and transport processes (e.g., Williams, 1989). Hysteresis refers to the asynchronous behavior between two processes, such as sediment and discharge and sediment and conductivity. As mentioned by a recent literature review by Liu et al. (2021), the processes and mechanisms behind hysteresis patterns are not fully understood. One common inference of sediment concentration versus discharge hysteresis is a clockwise pattern indicates an easily depleted sediment source lying proximal to the measurement point while a counter-clockwise pattern suggests a distal source from the measurement point (Williams, 1989; Lefrançois et al., 2007; Eder et al., 2010; Eludoyin et al., 2017; Zarnaghsh and Husic, 2021). Recently published, a fundamental study uses sediment continuity modelling with experiments and supports the proximal and distal inference for surface streams (Juez et al., 2021). However, the process-pattern linkage has primarily been applied to surface streams and remains under-studied for karst springs.

Sediment concentration versus electrical conductivity hysteresis may also be useful for inferring processes in karst because conductivity is often distinct for surface water and groundwater (Dahaan et al., 2016). Clockwise patterns are reported to indicate sediment resuspension in karst caves while counter-clockwise patterns indicate sediment deposition (Fournier et al., 2006; Schiperski et al., 2015; Valdes et al., 2006), however the linkage of the interpretation to processes has not been carefully examined. Sediment hysteresis applications and interpretation for karst systems have been generally limited to hysteresis being part of broader objectives to characterize various facets of karst systems. Lloyd et al. (2016) point out that hysteresis results from systems with fractures and caves can be of high complexity but a useful way to provide a cross comparison of different sites and events. Because karst springs differ so strongly from fluvial streams in their hydrologic controls, we hypothesize that the conventional interpretation of hysteresis patterns for karst will differ from that of surface systems.

The objectives were to (1) gain knowledge of karst sediment transport behavior, particularly with respect to internal versus external controls on loading and (2) advance interpretation sediment hysteresis patterns and their inference in karst basins. To meet these objectives, we analyze of a new dataset from sinking streams and phreatic cave sites for an epigenetic karst basin in the inner bluegrass region of Kentucky USA, carry out numerical modelling, and perform meta-analysis of published sediment datasets for karst.

2. Methods

2.1. Study site

The study site was the Cane Run watershed (62 km^2) and Royal Spring karst groundwater basin (58 km^2), located in the inner bluegrass region of central Kentucky, USA. The surface stream network of Cane Run Creek, which carries water and sediment during storm events, is densely packed with over 60 swallets (in-stream sinkholes) along its length (Husic et al., 2017a). These swallets partially redirect water and sediment to the subsurface karst system. Together, Cane Run and Royal Spring form a surface and sub-surface coupled drainage basin with mature karst development. A primary cave, approximately 5.5 m^2 in cross sectional area, drains groundwater to Royal Spring, which provides drinking water for the City of Georgetown (Fraley, 2019). Royal Spring is the largest perennial spring in the inner bluegrass region (Currens et al., 2015). This karst cave has been studied by many, including Husic et al. (2017a,b), and Al Aamery et al. (2021), providing evidence that the aquifer is always phreatic, while the overlaying epigenetic aquifer has varying levels of saturation. Phreatic conduits are very common and have been studied by White (2002), Drysdale et al. (2001), Massei et al. (2003), Herman et al. (2008), and others. A description of the soils and geology of the Royal Spring basin can be found in Husic et al. (2017a,b).

We chose five sampling locations (Fig. 1), including three surface sites in the Cane Run Creek network and two sites along the primary cave system. *Surface Site 1* and *Surface Site 2* drain urban and rural portions, respectively, of Cane Run Creek. *Surface Site 3* is situated at the outlet of upper Cane Run Creek watershed. The two cave sites are located in the longitudinal upper section of the cave, termed the *Upstream Cave Site*, and at the spring where the cave daylights, termed the *Downstream Cave Site* at Royal Spring.

2.2. Data collection and quality control

In situ pressure transducers were installed at *Surface Sites 1*, *2*, and *3* to collect water depth data in 10-minute intervals. A stage-discharge relationship was used to calculate the water flowrate values from the stage height recordings of the pressure transducers (Husic, 2015). At the *Upstream Cave Site*, a pressure transducer was installed in a monitoring well to measure stage and a stage-discharge relationship was established using velocity measurements in the conduit deployed temporarily in the well (Husic, 2015). The United States Geological Survey (USGS) gage station 032881100 provided flowrate data for the *Downstream Cave Site*.

Sensor platforms were used measure the turbidity and the electrical conductivity. Data were collected at the three *Surface Sites* and *Upstream Cave Site* using YSI 6920V2-2 multiparameter water quality sondes connected to Campbell Scientific CR 20 data loggers at a 10-minute resolution (Husic, 2015). Data were collected at the *Downstream Cave Site* using a YSI 6600V2 multiparameter sonde and a YSI 600 OMS V2 optical sonde connected to Campbell Scientific CR 1000 data logger.

Total suspended sediment (*TSS*) samples were used to establish relationships with turbidity so that continuous turbidity data could be used as a *TSS* surrogate (e.g., Walling et al., 2006). *TSS* samples were collected with Teledyne ISCO 6712 automated pump samplers during storm events. Grab samples were collected at approximately on a weekly basis at all locations. The samples were returned to the lab where they were processed through 0.45-μm Whatman filters to retain the sediment, and used to estimate sediment mass (USEPA, 1999). Surrogate relationships between *TSS* and turbidity were established with regression optimized through the data, separately for each site (Cao et al., 2021; Drysdale et al., 2001).

Quality control of data followed several steps detailed in Bettel (2021) and outlined here in brief. Water flowrate at the spring was corrected using data from the Georgetown Water Treatment Plant (GWTP) to account for their intake located upstream of the USGS gage. All instrumentation was checked weekly for power concerns, damage by flow events, electrical short-circuiting, or animals chewing on instruments, and data were downloaded and batteries switched at that time. The sensor probes and connecting cables were cleaned and calibrated following the steps of the manufacturer. Raw data at the spring were evaluated for erroneous data with the help of the *GCE Data Toolbox*, a software for metadata-based processing, analysis, visualization, and transformation of environmental data (Georgia Coastal

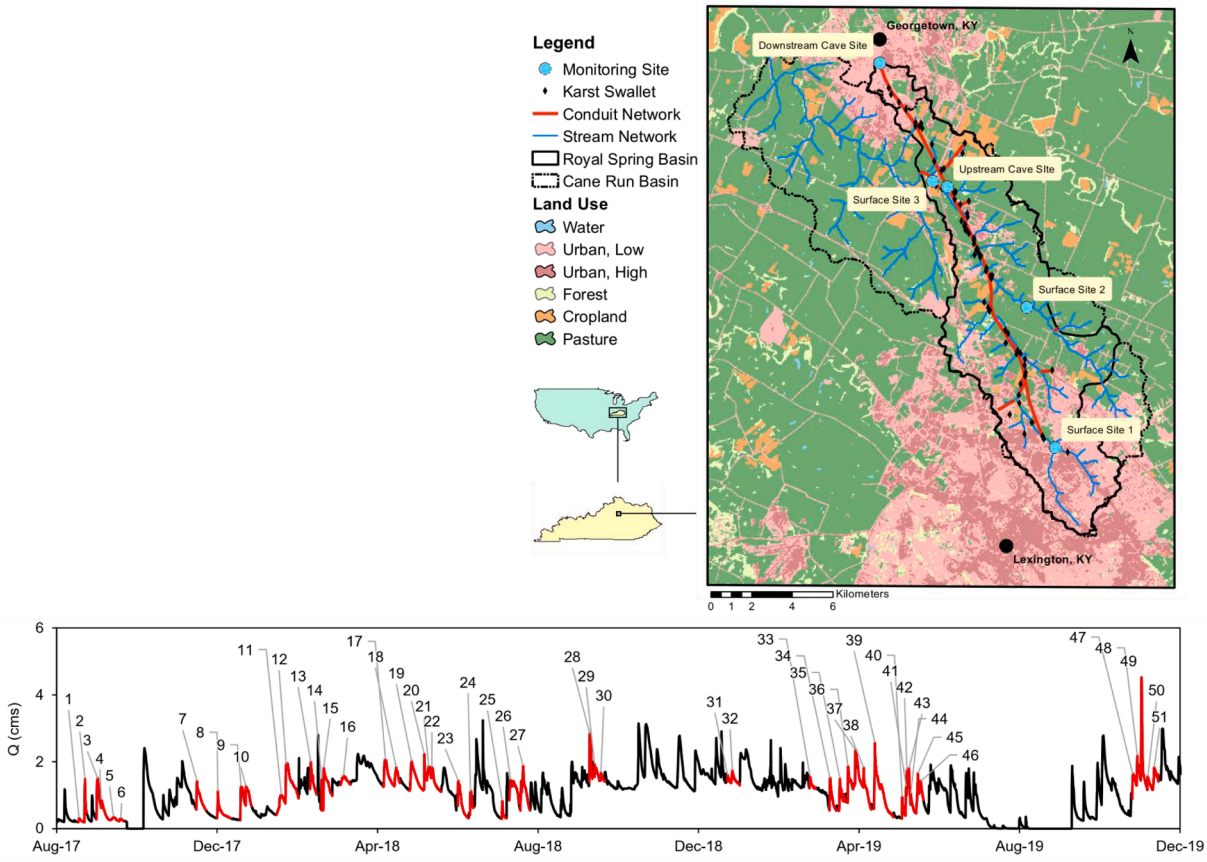

Fig. 1. Location Map of the Cane Run Watershed and Royal Spring Basin and Events Sampled (highlighted in Red). (For interpretation of the references to colour in this figure legend, the reader is referred to the web version of this article.)

Ecosystems LTER, n.d.) run in *Matlab* Version 2021b. The toolbox was applied to evaluate each data point for possible errors that arose during data collection. Categorization of problems associated with data included: 'invalid' data range, 'questionable' data not expected to be recorded but are physically possible under certain circumstances, 'percentage' for flagging data points for checking with a large change in their value, 'standard deviation' flagging to mark outliers in the dataset, and 'missing' data points for periods during which the datalogger was not supplied with power. During the quality control process, monthly data quality reports were completed and are archived in Clare (2019) and Bettel (2021).

2.3. Event analyses of data, hysteresis, and mixing modelling

We identified hydrologic storm events for periods during which all three parameters, discharge (*Q),* total suspended solids (*TSS),* and electric conductivity (*EC)* measurements were available (Fig. 1, sampled events highlighted in red). Events were manually extracted, starting at the point at which a pronounced increase in discharge was observed and ending when flow had returned to pre-event conditions or when a new event started. Each event was evaluated for its duration and the magnitude and timing of initial, peak, and ending values of *Q, TSS,* and *EC*. The parameters were each normalized by creating percentiles using their respective event maxima, so that cross-site and cross-event analyses could be carried out (Cao et al., 2021; Fournier et al., 2006; Lloyd et al., 2016). To further facilitate cross-event comparison, all sites were adjusted to a common time datum corresponding to $t = 0$ when the respective hydrographs reached their maximum flowrate. Event analyses included data from 25 h before the hydrograph peak to 75 h after the hydrograph peak. This event duration allows focus on the important information without omitting any substantial data associated with the precipitation events, as events do not typically show pulses in *Q, TSS,* or *EC* 75 h after the hydrograph peak (see Fig. S1). A few uncharacteristic events did show additional pulses at late time periods in the event, and these events were sampled during an in-stream construction operation in Cane Run Creek (see Fig. S2).

We carried out hysteresis analysis following visual and quantitative methods. The *TSS-Q* and *TSS-EC* hysteresis patterns were observed after plotting the normalized data. Several metrics commonly applied in hysteresis analyses were calculated for each event and then were evaluated separately and cumulatively (Liu et al., 2021; Zarnaghsh and Husic, 2021). *TSS* peak lag time was calculated as.

$$TSS_{lag} = t_{\max(Q)} - t_{\max(TSS)} \tag{1}$$

where $t_{\max(Q)}$ is the time at which Q reaches its maximum flow, $t_{\max(TSS)}$ the time at which *TSS* reaches its maximum concentration. The hysteresis index was calculated as.

$$HI = \sum \left(TSS_i^{RL} - TSS_i^{FL}\right)/n, \tag{2}$$

where *HI* is the hysteresis index of normalized discharge, TSS_i^{RL} is the normalized sediment concentration on the rising limb at percentile i, TSS_i^{FL} is the normalized sediment concentration on the falling limb at percentile i, and n is the number of percentiles i (Cao et al., 2021; Heathwaite & Bieroza, 2020; Lloyd et al., 2016). The flushing index (*FI*) was calculated as.

$$FI = \left(TSS_{\max(Q)} - TSS_{\min(Q)}\right)/\max(TSS), \tag{3}$$

where $TSS_{Q_{max}}$ is the total suspended solids concentration at Q_{max}, and TSS_{Q_o} is the total suspended solids concentration at the beginning of the event (Heathwaite & Bieroza, 2020). Histograms were plotted for *TSS*

lag times, *HI* and *FI* to investigate distributions, and the mode, mean, variance, skewness and kurtosis were calculated and analyzed.

We performed end member unmixing with *EC* as the tracer to separate the contribution of water sources in the aquifer from surface-derived runoff in the sinking streams and antecedent groundwater in the karst aquifer. *EC* has been deemed fairly conservative for surface and groundwater mixing during storm events (Massei et al., 2003; Pellerin et al., 2008). The solution is algebraic for two sources and one tracer as.

$$EC_i^T = EC_i^B X_i^B + EC_i^R X_i^R \quad and \tag{4}$$

$$X_i^B + X_i^R = 1, \tag{5}$$

where EC^B is the conductivity of the baseflow groundwater, EC^R is the conductivity of the runoff, and EC^T is the total conductivity at timestep *i*, and *X* indicates the mass fractions. The mass fractions use the ratio of volumetric flowrates for incompressible flow as.

$$X_i^B = Q_i^B / Q_i^T, \tag{6}$$

$$X_i^R = Q_i^R / Q_i^T, \tag{7}$$

where Q_i^T is the total averaged flow at timestep *i*, Q_i^B is the baseflow at timestep *i*, and Q_i^R is the stormflow at timestep *i*.

We carried out hysteresis loops for the unmixed signal, including runoff and *TSS* concentrations at each site. We plotted Q^R against the *TSS* concentrations for the 15-minute intervals identified looping direction.

2.4. Fluvial erosion modelling in the cave

We modelled fluid shear stress (τ_f), sediment flux (Q_{ss}), and commonly reported fluvial erosion formula for the cave. The analysis was carried out to investigate potential evidence that fluid shear stress in the cave controls sediment flux of internally sourced sediment transported through the cave. Fluid shear stress was modelled using the Darcy–Weisbach approach as.

$$\tau_f = \frac{1}{8} f \rho V^2, \tag{8}$$

where the fluid shear stress (τ_f) is in Pa, f is the Darcy–Weisbach friction factor and is dimensionless, ρ is the fluid density (kg m^{-3}), and V is the bulk streamwise velocity through the cave (m s^{-1}). The friction factor was parameterized for the primary cave of the Royal Spring groundwater basin in Husic et al. (2017b) and was carried forward herein. Velocity was estimated every 15 min using the USGS measurements for water flowrate and approximation of the cave's bathymetry. The shape of the underground cave was estimated as elliptical based on our previous research of the spring, and the elliptical long diameter was estimated as 6 m while the elliptical short diameter was 0.9 m. This estimate is based on a great deal of historic research of the cave bathymetry over the past 40 years by the Kentucky Geological Survey (KGS) and researchers at the University of Kentucky. Dye tracers were used to find connectivity of the cave system across the extent as well as travel time for different hydrologic conditions within the cave by Spangler (1982), Taylor (1992), and Paylor and Currens (2004). Thrailkill and Gouzie (1984) investigated linear velocity, cave geometry, and conveyance in the conduit, and Tripathi (2009) used electrical resistivity to determine the footprint of the cave. The KGS used down-hole images in combination with Doppler sonar instruments to determine the approximate geometry of the conduit (Husic, 2015). The combined results of the mentioned methods made it possible to estimate the general shape of the cave, which was estimated as an elliptical conduit (i.e., an average short diameter in the vertical direction of 0.9 m and an average long diameter in the transverse direction of 6.2 m, Husic, 2015; Husic et al., 2017a,b). Sediment flux was estimated every 15 min using the sediment sensor and water flowrate measurements.

The potential of the fluvial erosion process controlling erosion of internal sediment in the cave and in turn controlling sediment flux was assessed using the fluvial erosion formula of Partheniades. The Partheniades equation is a widely used erosion and resuspension formula for cohesive sediment and is given as.

$$\varepsilon = A_{eff} k_d \left(\tau_f - \tau_c\right)^M, \tag{9}$$

where ε is the sediment flux *via* the fluvial erosion process (g/s); A_{eff} is a supply term defined as the effective area of the cave bed supplying sediment (%); k_d is the erodibility coefficient; τ_c is the critical shear stress (Pa); and M is the erodibility exponent and is near 1. The erodibility coefficient was parameterized as a function of τ_c following the work of Hanson and Simon (2001). The effective area reflects the concept that some portions of the cave bed are covered with fluvial sediment and other portions of the bed are bedrock with no available fluvial sediment. In this way, the potential to adjust A_{eff} for different conditions was investigated.

2.5. Numerical modelling of sediment pulses in the karst aquifer

Numerical modelling using the conservation of mass for water and sediment was carried out to simulate the effect of an externally sourced sediment pulse that enters the subsurface and transports through the aquifer and cave system during a storm event. A sediment pulse from the sinking streams was input using the sediment concentration data. Water and sediment routing through the upper aquifer was accomplished *via* a reservoir model approach for the system (e.g., Husic et al., 2019). Routing through the cave system was accomplished by discretizing the cave and treating the system as pipeflow (e.g., Husic et al., 2017b; Al Aamery et al., 2021). The model was formulated for the karst aquifer as a reservoir and the cave system as.

$$\frac{dS_{res}}{dt} = Q_{sw} + Q_{gw} - Q_{cave-in}, \tag{10}$$

$$\frac{d(TSS_{res}\, S_{res})}{dt} = TSS_{sw} Q_{sw} + TSS_{gw} Q_{gw} - TSS_{cave} Q_{cave-in}, \tag{11}$$

$$\frac{dS_{cave}}{dt} = Q_{cave-in} - Q_{cave-out}, \text{ and} \tag{12}$$

$$\frac{d(TSS_{cave}\, S_{cave})}{dt} = TSS_{cave-in} Q_{cave-in} - TSS_{cave-out} Q_{cave-out}. \tag{13}$$

The first two equations were setup for the karst aquifer reservoir that is modelled as an unsteady flow detention basin and the second two equations are for the phreatic that is modelled as pipeflow. *S* and *TSS* indicate water storage (m^3) and sediment concentration (g l^{-1}); and subscripts *sw*, *gw*, *cave-in*, and *cave-out* indicate swallet water from the sinking streams, groundwater recharge from the fracture flow and phreatic matrix draining the soil and epikarst, cave water inputs, and cave outputs, respectively.

Parameterization of model fluxes and model discretization was accomplished using commonly applied karst reservoir routing formula and conduit approaches (Hartmann et al., 2014; Husic et al., 2017b; 2019). A reservoir approach was applied to both the exit from the karst aquifer to the cave and the groundwater recharge from fractures and the rock matrix as.

$$Q = \alpha S_{res}^{\beta}, \tag{14}$$

where α and β are reservoir coefficients. The storage in the karst aquifer was treated as the product of the reservoir depth and effective area ($S_{res} = H_{res} A_{eff}$). A constant value was applied for the sinking streams net water flowrate recharging the karst aquifer via the swallets, and this input was adjusted to zero when the karst aquifer was saturated. These

assumptions are reasonable given the 50 plus swallets for which subsequent filling and overtopping has been observed in the creek system. The equations were discretized in time and one reservoir was used for the system following the work of Husic et al. (2019), and five cave segments were modelled. The unsteady terms were set to zero in the cave since the cave is always phreatic, and therefore the water flowrate at the spring was useful to set initial conditions for the karst aquifer. Coefficients of the reservoir fluxes, the effective area of the aquifer were adjusted to agree with mean water flow rate conditions at the cave's spring. Sediment concentration from the sinking streams entering the

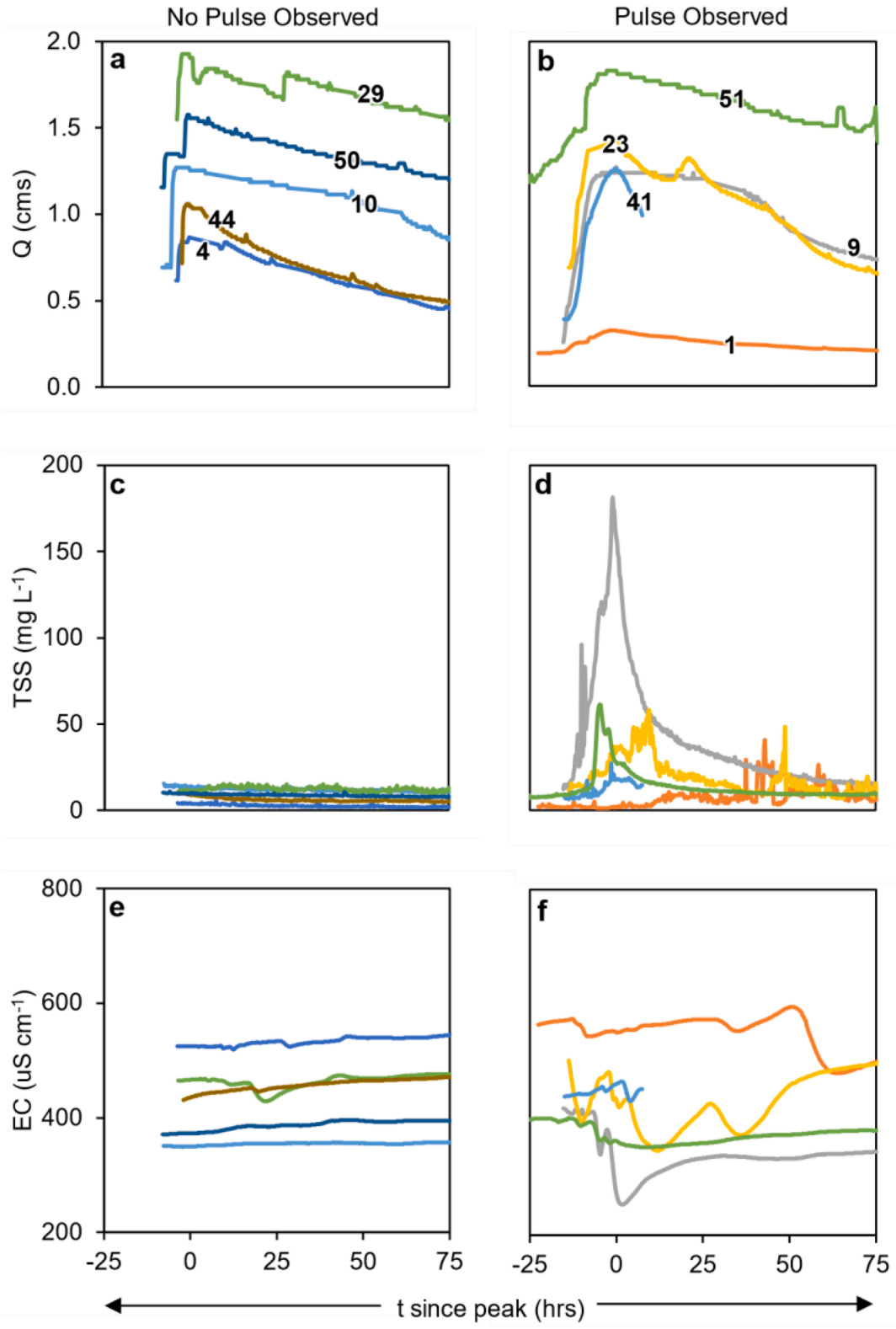

Fig. 2. Examples of results for events where TSS pulse was not observed or the pulse was observed. (a-b) Average *Q* (c-d) Average *TSS* (e-f) Average *EC* (g) comparison of events as a function of *Q* range and maximum *Q*.

aquifer via swallets was set to match the surface stream sediment concentration mean distribution given the relative similarities across events. Sediment deposition and erosion in the cave were assumed to be equal in amount and therefore were not included in the simulations so that we could isolate impacts of mixing the sediment-laden surface-derived water with the clear-water groundwater in the aquifer and observe the constraint on water discharge in the cave that slows the transport velocity.

3. Results

3.1. Internal and external sources of sediment during events

Results from data collection at Royal Spring produced 51 individual hydrologic events with coinciding turbidity and conductivity data (Fig. 1). Despite hydrograph responses at the spring, 10 events had no pronounced pulses of *TSS* or *EC* and two events showed irregular behavior and were difficult to interpret (Fig. 2). The remaining 39 events showed pronounced *TSS* and *EC* pulses in temporal proximity to *Q* peaks (Fig. 2). Close examination of the 10 sedigraphs with no observable pulses showed *TSS* experienced a slight increase and then decreased with the rising and falling limb of the hydrograph (Fig. 2). However, this dependence was very low in comparison to other 39 events that exhibited a noticeable sediment pulse. The sediment pulses occurred in conjunction with the hydrograph response, albeit at times out of phase with *Q*, and included a steep incline in *TSS*, peaking which was then followed by a decrease to pre-event *TSS* conditions.

We examined factors controlling the presence or absence of sediment pulses observed at the spring for the 39 and 10 events, respectively. The peak water flowrate for each event, as measured at the spring, showed no significance as a factor controlling the classification of events as showing the presence or absence of the sediment pulses (p-value = 0.21, two-tail *t*-test assuming unequal variances). However, the hydrograph range (Q_{Range}) clustered to two types of event and significantly controlled classification of the events as showing the presence or absence of sediment pulses (p-value = 0.005). Q_{Range} is defined as the difference between the peak water flowrate and the pre-event flowrate for each individual event. Eight of the 10 events with no *TSS* and *EC* pulse had a Q_{Range} less than 0.5 cms while 32 out of 39 events with *TSS* and *EC* pulse had a Q_{Range} greater than 0.5 cms. The clustering metric is not absolute, but Q_{Range} does separate 82 % of the events and suggests an underlying hydrologic process.

We attribute the absence of pulses in the sedigraphs and chemographs (Fig. 2, left column) to saturated conditions for the karst aquifer at the start of the event. A pre-event condition of saturated aquifer prevents externally sourced sediment transported into the aquifer by preventing high *TSS* runoff water from entering the cave. The surface streams overtop the swallet openings and, in turn, a relatively small increase in water flowrate is observed at the spring (i.e., <0.5 cms increase in *Q* at Royal Spring). This interpretation is consistent with the *EC* distribution. On the other hand, the presence of pulses in the sedigraphs and chemographs (Fig. 2, right column) provide evidence that externally sourced sediment has entered the cave. Events with the presence of an *EC* pulse show a sharp decrease of *EC* consistent with recharge from the surface streams to the karst aquifer. The results suggest that only sediment internal to the karst cave was transported during events with no *TSS* or *EC* pulse, while both internal and externally-derived sediment was transported to Royal Spring during events with *TSS* and *EC* pulses.

Fluvial erosion modelling results for the cave supported the separation of the 10 events with no *TSS* and *EC* pulses and 39 events with pulses as internal sediment only and combined internal-external sediment, respectively (Fig. 3). Sediment flux estimated from the measured data (Q_{ss}) is plotted as a function of fluid shear stress in the cave (τ_f) for the 10 events with no *TSS* and *EC* pulse (Fig. 3a) and for data from a sample of events with pulses (Fig. 3b). Sediment flux shows a direct dependence on fluid shear stress in the cave for the events with no *TSS* and *EC* pulses. We interpret this result to reflect the process of fluvial erosion in the cave in which fluid shear stress at the floor of the cave causes internal sediment transport. Sediment flux shows a dependence on fluid shear stress in the cave for some of the data collected for events with pulses. However, the majority show clustering and scattered behavior with no clear dependence on shear stress in the cave. We interpret this result to reflect mixed processes of fluvial erosion in the cave and sediment influx to the cave through swallets from the sinking streams indicating both internal and externally-sourced sediment transport. We plot the fluvial erosion formula modified from Partheniades *via* the work for silt-sized sediment by Hanson and Simon (2001). The fluvial erosion formula was optimized well for data from events that showed no pulses in Fig. 3a. However, much of the data in Fig. 3b does not agree with the fluvial erosion formula owing to the interpretation that this is externally-originated sediment that moves through the system as a pulse of sediment.

3.2. Time-series results

Time-series results for events with sediment pulses showed a shift in behavior longitudinally in the basin from surface sites to Royal Spring, indicating increased water and sediment retention. The longitudinal

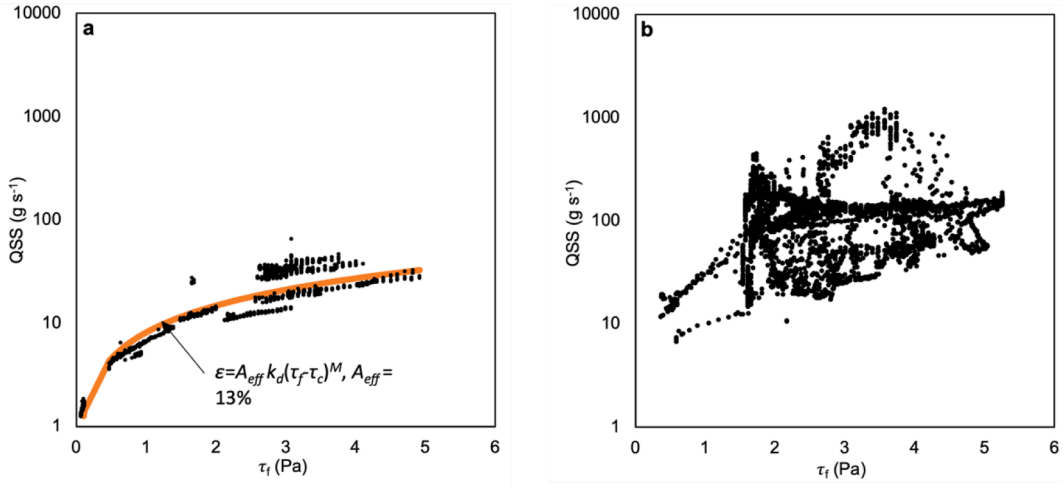

Fig. 3. Sediment flux, Q_{ss}, at the downstream cave's spring plotted as a function of fluid shear stress in the cave, τ_f. (a) Data from events with no pulses and fluvial erosion formula, (b) data from events exhibiting pulses.

trends are seen when observing hydrographs (*Q* versus time), sedigraphs (*TSS* versus time), and chemographs (*EC* versus time) data from the Cane Run streams, the upper cave site, and downstream cave site at Royal Spring (Fig. 4). The mean distributions (dashed black lines in Fig. 4 a-e) show the base of the hydrograph widens, reflecting increased residence time of surface-derived runoff and in turn longer duration events moving from upstream to downstream. The time-series at *Surface Site 1* shows the sharpest hydrograph peak and the narrowest base, followed by *Surface Site 2*, *Surface Site 3*, *Upstream Cave Site*, and, with the widest base, the *Downstream Cave Site*. For the surface streams, the shifts are expected because of an increase in drainage area across the three locations. For the cave, the longer duration hydrographs and sedigraphs reflect an increase in water and sediment retention time with some events showing the cave hydrographs extending an order of magnitude longer than the duration of hydrographs in the surface streams. The water velocity in the cave is on average 16 % of the water velocity in the surface streams. This result agrees with water conveyance estimates in the karst aquifer, and conveyance is greatly reduced in the cave relative to the surface streams because the cave experiences pipeflow mechanics and thus is limited in its cross section (Al Aamery et al., 2021).

Sediment concentration and electrical conductivity time-series results from the cave sites point toward externally sourced sediment and water. The sedigraphs and chemographs show consistent pulses during the events. The mean sedigraph pulses at each site (dashed black lines in Fig. 4 f-j) had a general inverse agreement with the mean chemograph pulses (dashed black lines in Fig. 4 k-o). The surface sites show primary sediment pulses attributed to surface erosion and sediment transport as runoff is generated. *Surface Sites 2* and *3* show secondary pulses attributed to streambank erosion in the main corridor, as these sites show the greater height of streambanks and experienced degradation the past decade (Bettel, 2021). The chemographs show pronounced negative pulses at surface sites consistent with the observation that *EC* of runoff in surface streams is typically considerably lower than that of groundwater (e.g., Dahaan et al., 2016). These transfers of water and sediment to the subsurface karst are visually evident as primary pulses are observable, although elongated in duration due to the previously mentioned increase in residence time. Instantaneous sedigraph results at Royal Spring (colored lines in Fig. 4j) showed examples of observed primary and secondary pulses attributed to surface and bank erosion transferred from the sinking streams.

3.3. TSS-Q hysteresis

Results of hysteresis patterns and metrics for sediment concentration as a function of water flowrate (*TSS-Q* hysteresis) show a shift in behavior from clockwise patterns for the surface stream to figure eight at the upstream cave site to counter-clockwise patterns and very high variability at Royal Spring (see mean loops and instantaneous loops in Fig. 5). Out of the 39 events that showed *TSS* and *EC* pulses, visually 19 were clearly counter-clockwise, 0 were clearly clockwise, 5 events were a figure eight pattern showing clockwise and counter-clockwise loops, 9 events appeared linear, and 6 events showed complex patterns that were difficult to summarize. Of the 39 events, 29 events showed a positive TSS_{lag} indicating more counter-clockwise behavior, 8 events showed a negative TSS_{lag} indicating clockwise hysteresis, and two events showed a TSS_{lag} equal to zero indicating linear behavior. The mode of the TSS_{lag} shifts from −5 h to +5 h for surface streams to the cave, indicating a shift to counter-clockwise behavior at Royal Spring (Fig. 6). The central mode of the hysteresis index (*HI*) shifts from 0.3 for surface stream sites to 0.15 at the upstream cave site to −0.15 at Royal Spring, where a negative *HI* indicates counter-clockwise. The central mode for the flushing index shifts from 0.85 for the surface stream sites to 0.6 for the upstream cave site to 0.2 at Royal Spring. The flushing index indicates the system shifts from an almost exclusive concentration response at the surface to a mixed concentration and dilution response at Royal Spring. Variability of hysteresis shows that *HI* ranges from −0.4 to 0.3 at Royal Spring, demonstrating that various degrees of counter-clockwise and clockwise patterns that reflect the varying arrivals of *TSS* pulses.

Surface streams are reported to most often show clockwise patterns for *TSS-Q* hysteresis (Hamshaw et al., 2018; Cao et al., 2021) and our

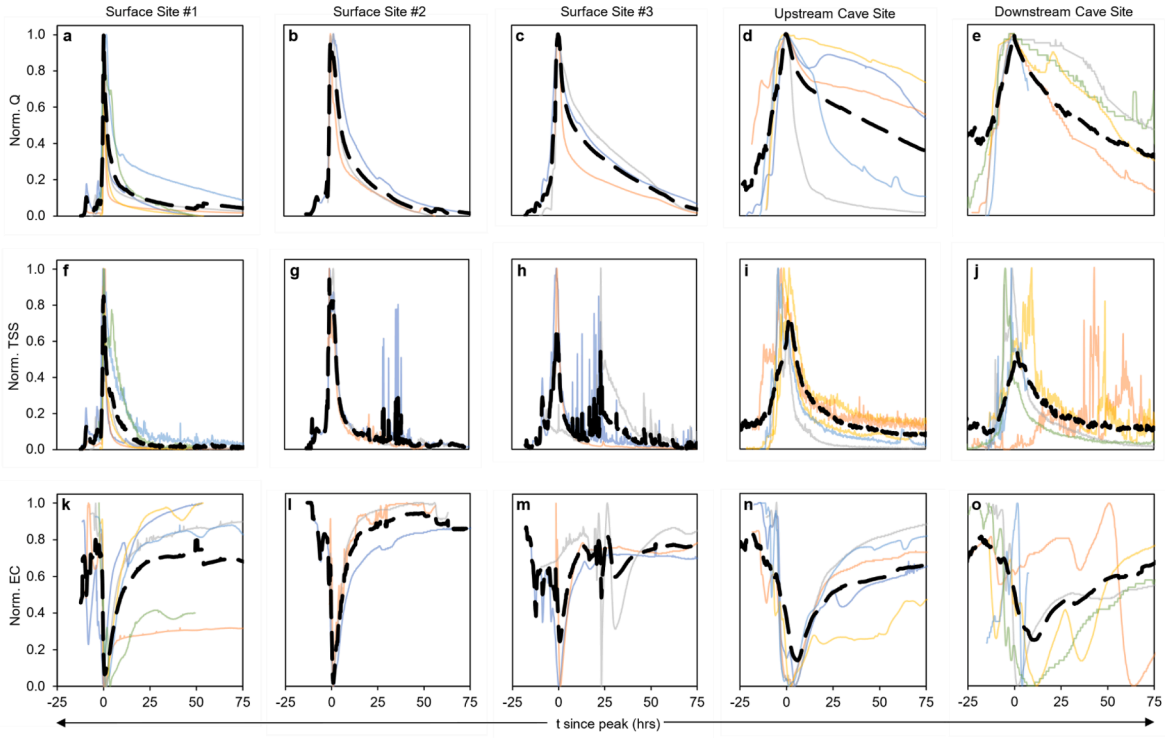

Fig. 4. Averaged Time Series (dashed black) Colored lines show examples of individual events at each site (a-e) Average Normalized *Q* (f-j) Average Normalized *TSS* (k-o) Average Normalized *EC*.

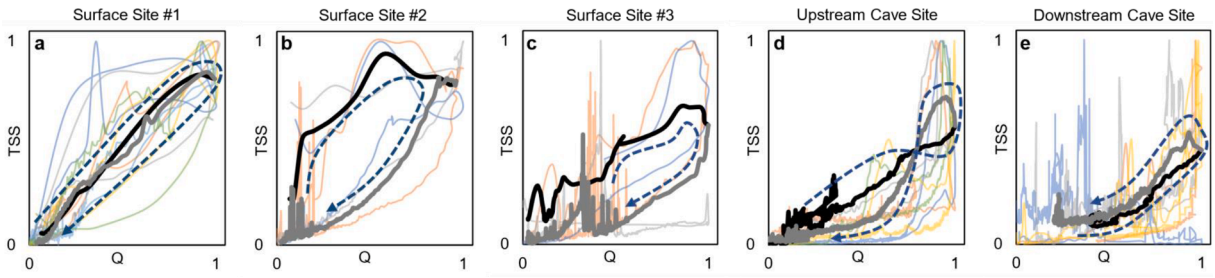

Fig. 5. Averaged *Q-TSS* Hysteresis (black) Colored lines show examples of individual events at each site, Solid black lines indicate rising limb of hydrograph, dashed black lines indicate falling limb of hydrograph.

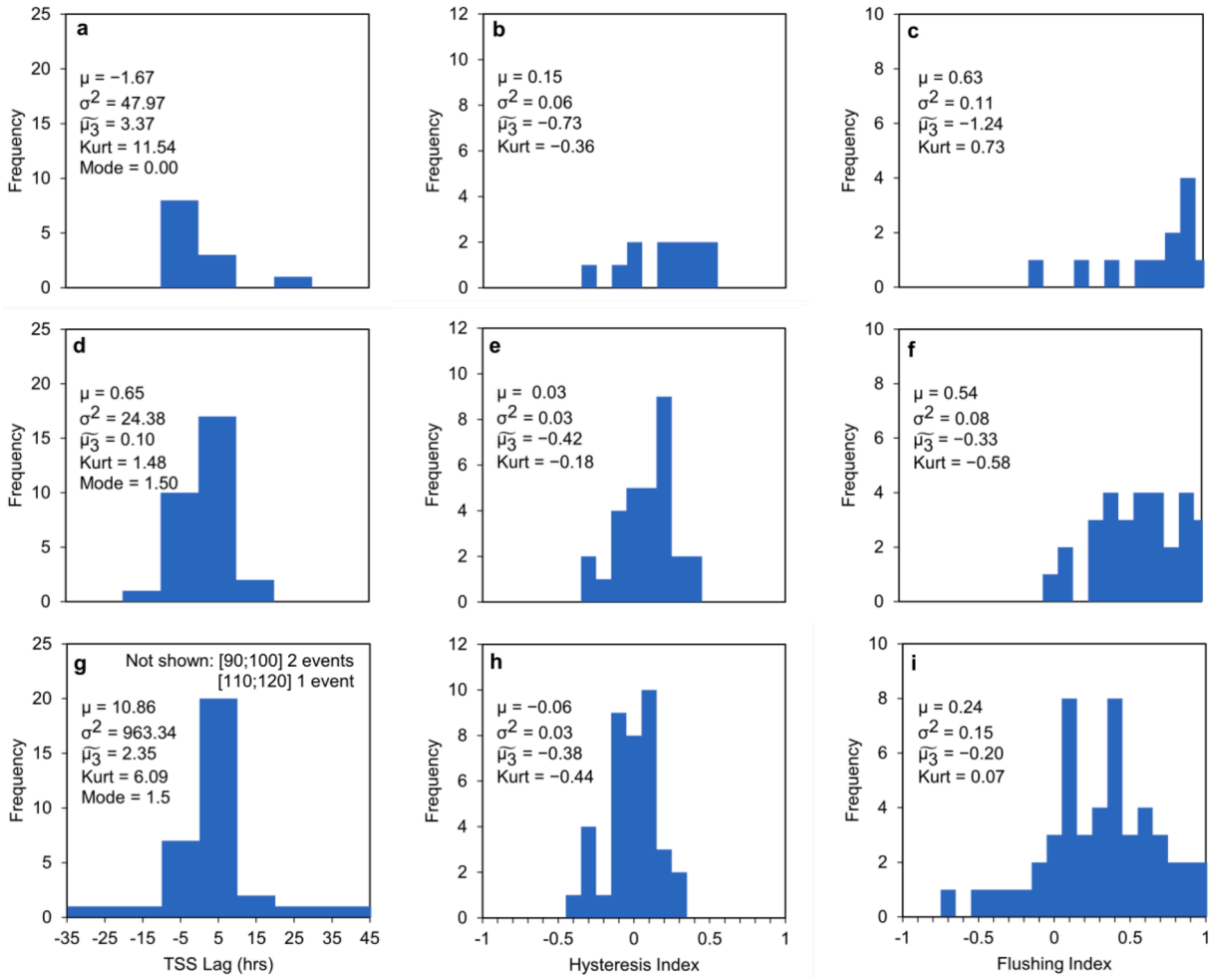

Fig. 6. Histograms for *TSS* Lag, Hysteresis Index and Flushing Index at (a-c) Surface Streams, (d-f) Upstream Cave Site, (g-i) Downstream Cave at Spring.

results in the Cane Run stream network agrees with this result. Clockwise hysteresis patterns are typically interpreted as erosion of proximal (close-by) sediment sources that are easily transported during a hydrologic event (Cao et al., 2021). In surface streams, the clockwise pattern is common because the sediment sources are close to the measurement location of the instrument, causing the sediment peak to occur early in the event, before the hydrograph peak. (Lloyd et al., 2016) This interpretation is reasonable for the surface streams of Cane Run Creek because the primary sediment source is stored sediment in the ephemeral network which is entrained during the rising limb of the hydrograph.

The shift to commonly shown counter-clockwise pattern with high variability for *TSS-Q* hysteresis at karst spring are unique results to the literature, and counter-clockwise patterns are less commonly reported for sediment hysteresis (Hamshaw et al., 2018, Krajewski et al., 2018, Lloyd et al., 2016) although some work has shown that intense urbanization pushes streams toward counter-clockwise behavior (Zarnaghsh and Husic, 2021). The common interpretation of counter-clockwise patterns for *TSS-Q* hysteresis is dominance of sediment transport from distal (far away) sediment sources that are not well connected to the measurement location of the instrument (Juez et al., 2018; Zarnaghsh and Husic, 2021). However, this interpretation may not hold for sediment hysteresis in karst caves. The hysteresis in the cave varies between clockwise and counter-clockwise, depending on events, with net counter-clockwise behavior. This behavior is likely a function of pre-event water storage in the karst aquifer.Numerical modeling results

and comparison with data support the dependence of counter-clockwise and clockwise hysteresis on the pre-event water storage in the aquifer. The data and numerical modeling results show that the modelled variation of the TSS_{lag} as a function of the time for the rising limb of the hydrograph (T_{RL}), in which the latter can be used as a surrogate to determine pre-event water storage conditions within the aquifer (Fig. 7a-b). High T_{RL} occurs because the aquifer is initially unsaturated and takes a long time to fill, while low T_{RL} occurs because the aquifer is initially near saturation and takes a shorter time to fill. The saturation state of the aquifer as a function of the rising limb time is illustrated in Fig. 7. When simulated as initially unsaturated (i.e., near empty, Fig. 7c), the aquifer takes approximately 60 h to fill with water and for the water flowrate to reach its peak flow (i.e., time for rising limb, T_{RL}). When simulated as initially saturated (i.e., near full, Fig. 7d), the aquifer takes approximately 10 h to fill with water and for the water flowrate to reach its peak flow (i.e., time for rising limb, T_{RL}). This result is consistent with conceptualizing the karst aquifer as a reservoir with the primary phreatic cave as the reservoir outlet.

The consistent behavior of the saturation states on sediment transport was also shown via the modelling (i.e., Fig. 7 sediment results). Storm events with an initially saturated aquifer, and thus short T_{RL}, have longer and net positive TSS_{lag} times, while events with an initially unsaturated karst aquifer show long T_{RL} and negative TSS_{lag} times. This concept can be seen visually in time series results from the numerical model of Fig. 7c, where sediment transport occurs for an event with an initially unsaturated karst aquifer—the *TSS* peak occurs before the hydrograph peak similar to a surface stream. Fig. 7d shows the modeling results for an event with an initially saturated aquifer—the sediment peak response is delayed due to the transport of clear water to the spring and pressure response of the system. For the nine data points on the top shown in Fig. 7a, we qualify that there is no visual dependence of TSS_{lag} on T_{RL}. These events occurred during the months from February to September 2018 when stream restoration contractors were restoring an approximately 1.6 km reach of the streambanks in the upper portion of the Cane Run Creek. This restoration activity intersected with the rain events of springtime 2018, which was the wettest year on the 150-year precipitation record from 1870 to 2020 (Bettel, 2021). The very high TSS_{lag} values are attributed to streambank erosion on the falling limb of the surface hydrographs during this time period (Fig. 4j, Bettel, 2021).

Results suggest the *TSS-Q* hysteresis for the karst cave is a function of the pre-event water storage of the aquifer. This contradicts the idea that the system shifts from proximal to distal sources. Royal Spring shows both counter-clockwise and clockwise behavior for different events (Fig. 6), and both patterns reflect the same external source of sediment from the sinking streams that is transported through the cave. The arrival of the sediment pulse is interpreted as a function of the initial

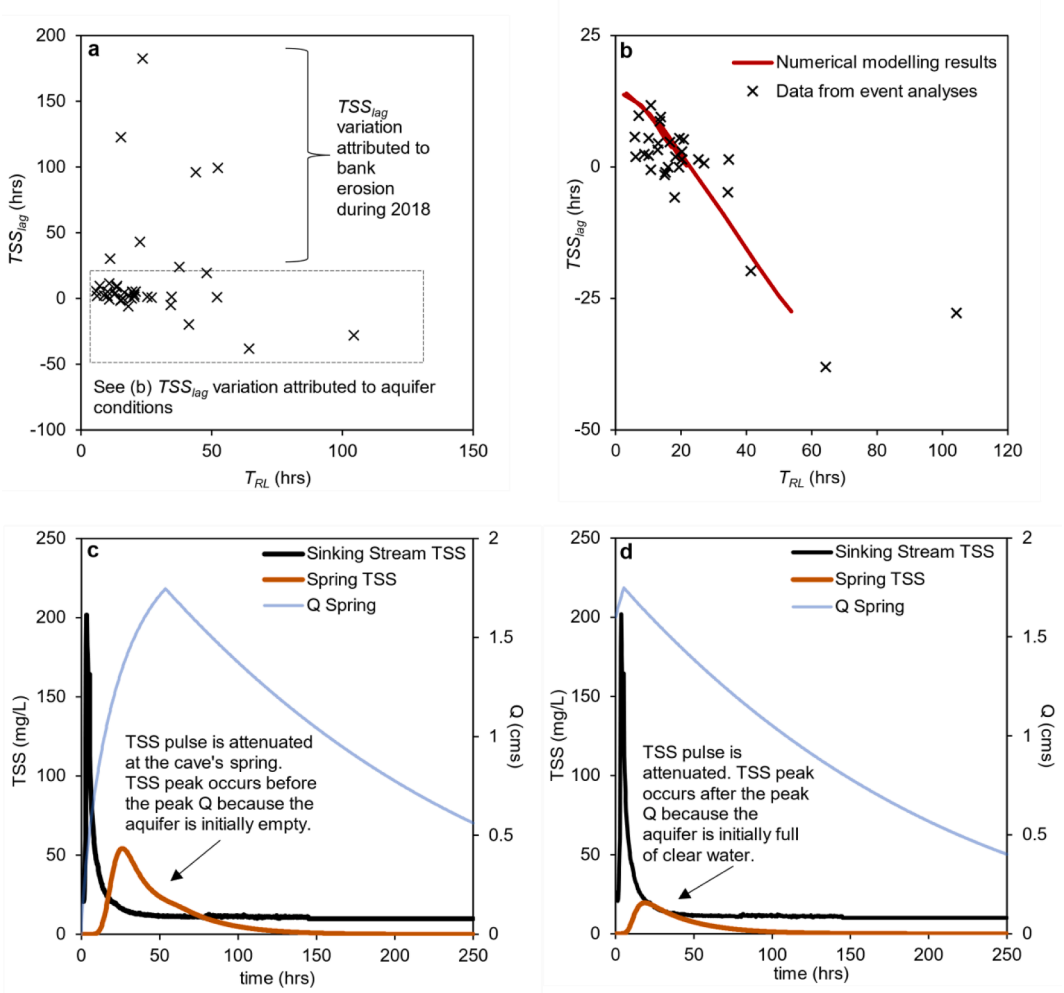

Fig. 7. Dependence of externally sourced sediment transport on aquifer initial conditions shown with data and numerical modeling (a) The lag-time of the suspended sediment peak (TSS_{lag}) at the cave's spring plotted versus the time duration for the rising limb water flowrate (T_{RL}) for the hydrograph at the cave's spring. (b) Data and numerical modeling results for variation of TSS_{lag} as a function of T_{RL} attributed to storage conditions of the aquifer. (c) Numerical modeling results showing the attenuation of an externally sourced sediment pulse for an initially empty aquifer. (d) Numerical modeling results showing the attenuation of an externally sourced sediment pulse for an aquifer initially near full of clear water.

water storage in the aquifer as opposed to the spatial location of the source. An aquifer that is initially unsaturated, or dry, will show arrival of the *TSS* pulse prior to Q_{peak}, and exhibit clockwise behavior similar to a surface stream. An aquifer that is nearly saturated will show a *TSS* pulse after Q_{peak} and exhibit counter-clockwise behavior because the pressure response of the pre-stored clear aquifer water arrives at the spring prior to the *TSS* pulse.

3.4. TSS-EC hysteresis results

Results of sediment concentration and electrical conductivity, *TSS-EC*, hysteresis provide evidence about the sources of water and sediment in the surface streams and the cave. Clockwise *TSS-EC* hysteresis loops occurred for all sites, including the cave and spring sites (Fig. 8 a-e). The main mode of sediment transport is from runoff water that arrives at each site, causing the *EC* values to drop as well as the *TSS* values increase. We also used mixing analyses for water sources and carry out hysteresis, and the hysteresis analyses of *TSS* and surface runoff support the *TSS-EC* hysteresis interpretation. The general trend from the upstream surface sites to the downstream cave site is that as the sites move further down, and the amount of runoff (Q_R) at the total hydrograph (Q_T) peak decreases. This trend is observed for the runoff (Q_R) contribution at the *TSS* peak time: the further downstream in the cave the site is located, the less runoff is contributing to the total flow at the time the *TSS* peak occurs. Regardless, the *TSS*-Q_{Runoff} hysteresis loops are consistently clockwise patterns and agree with the *TSS-EC* results.

The *TSS-EC* hysteresis is valuable because it isolates the water's runoff origin and relationship to the sediment. Results provide evidence that all sediment pulse are from the same source—external sediment that transports to the subsurface karst from the sinking streams. In this manner, the *TSS-EC* hysteresis removes the effect of the pre-event storage of water in the karst aquifer and shows that sediment is not distal or proximal. In all cases, the *TSS* peak occurs before the *EC* peak because the *TSS* pulse occurs during the rising limb of the runoff hydrograph as entrainment occurs at the surface.

4. Discussion

4.1. Sediment transport in karst

Results lead to a conceptual model for behavior of sediment transport in the phreatic karst system and interpretation of hysteresis patterns (Fig. 9). Three modes of sediment transport behavior in the karst cave are conceptualized, including (1) internal sediment transport with no hysteresis at the spring, (2) externally sourced sediment transport with counter-clockwise hysteresis, and (3) externally sourced sediment transport with clockwise hysteresis. All three modes of sediment transport are hypothesized to be a function of initial water storage in the karst aquifer as indicated with saturated and unsaturated rock matrices. These aquifer conditions include initially saturated, initially partially saturated, and nearly empty of water initially. The unsteady sediment arrival to the aquifer also controls externally sourced sediment transport in modes two and three.

The first mode of sediment transport in the karst cave is internal sediment transport only with no hysteresis at the spring (top panel in Fig. 9), and this mode is attributed to the karst aquifer that is initially full of water. The initial, fully saturated rock matrix leads to the surface stream overtopping the swallets. Sediment-laden water cannot enter the karst aquifer, however the increased free surface of the surface stream associated with the flood wave causes an increased hydraulic head for the aquifer. In turn, the water flowrate in the cave is increased, as is the fluvial shear stress. This condition leads to internal fluvial erosion of sediment from the bed of the cave. At the spring, the hydrograph shows a slight increase in flowrate that is mirrored by the sedigraph and no hysteresis loop occurs.

The second and third modes of sediment transport reflect the unsteady arrival of sediment from external surface streams and the pre-event water storage of the aquifer. The surface stream sedigraph

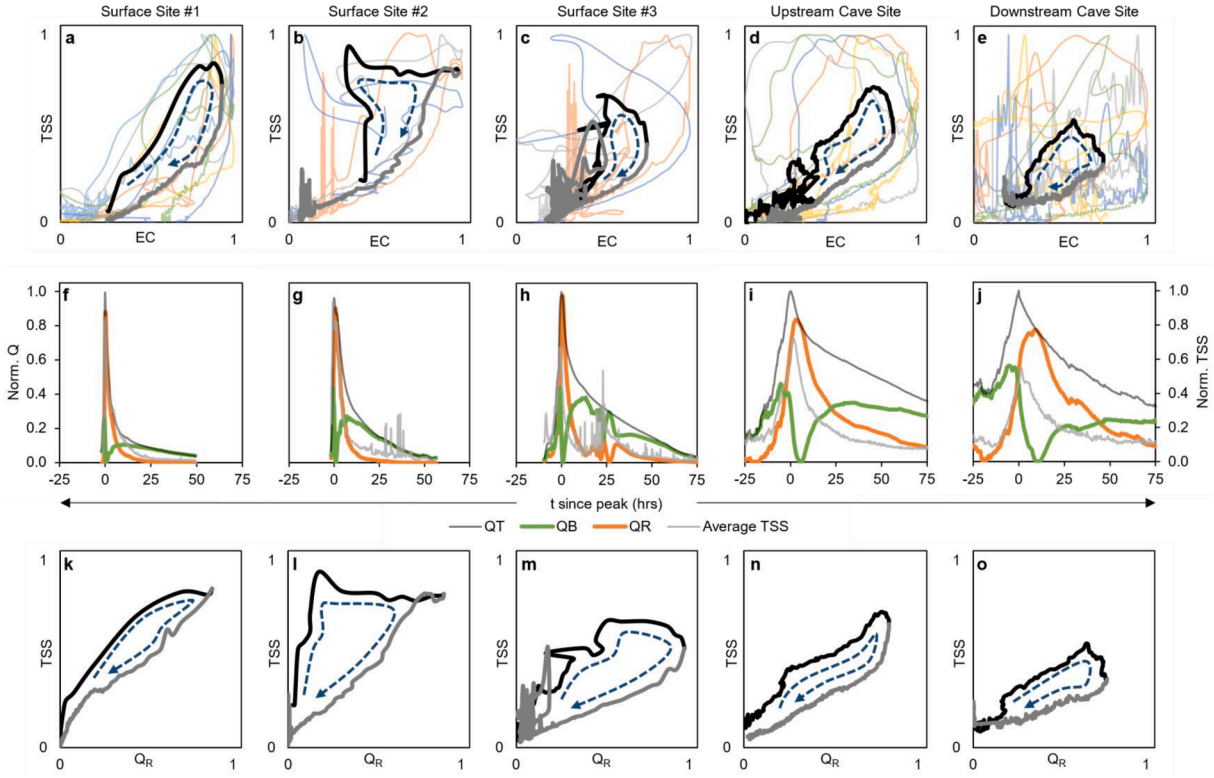

Fig. 8. Averaged *EC-TSS* Hysteresis (black) Colored lines show examples of individual events at each site. Solid black lines indicate falling limb of chemograph. Dashed black lines indicate rising limb of chemograph.

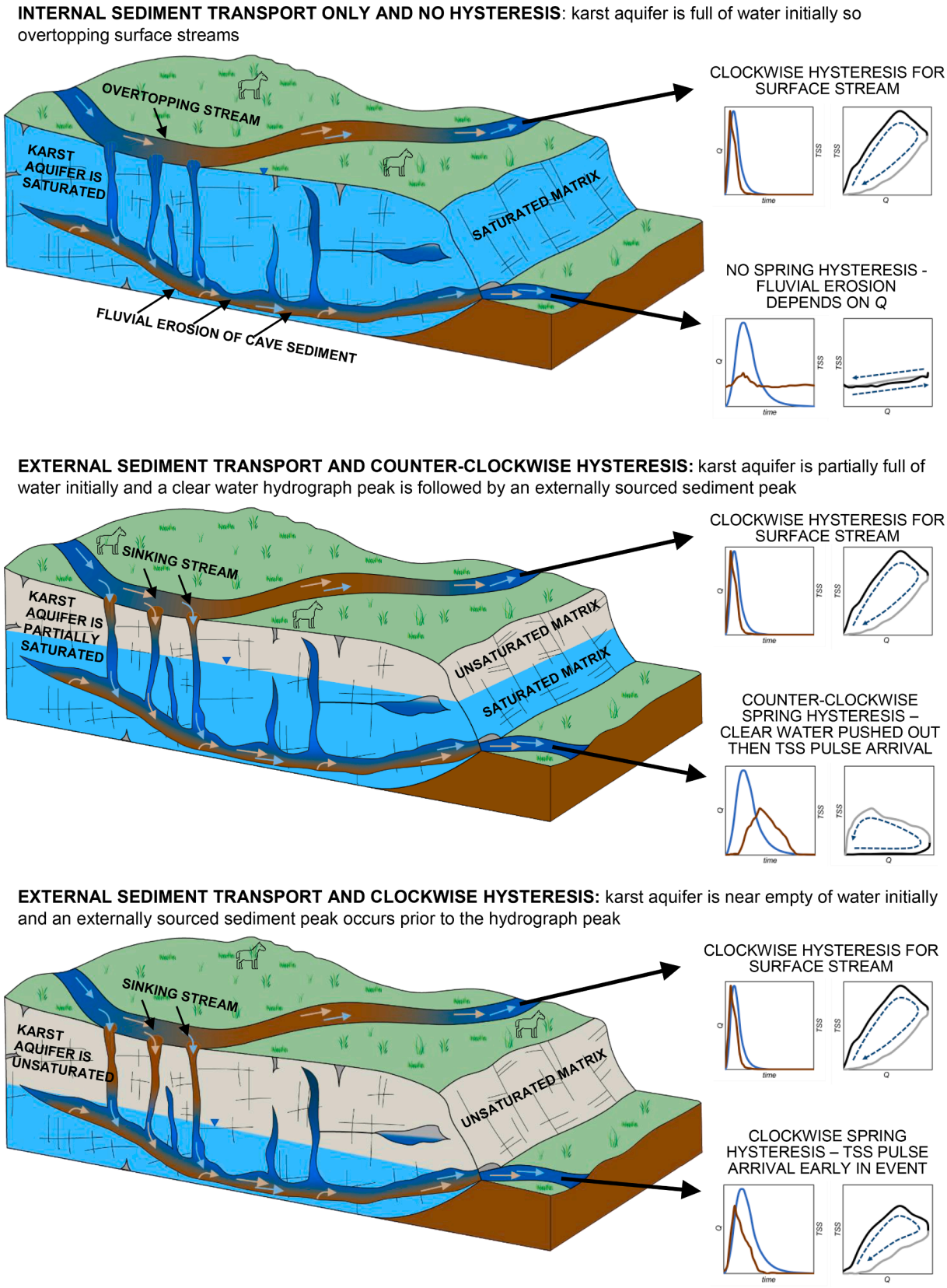

Fig. 9. Concept of pre-event conditions impacting hysteresis in karst. Colors are defined such that dark blue is low sediment water and brown is sediment laden water. (For interpretation of the references to colour in this figure legend, the reader is referred to the web version of this article.)

shows increasing sediment concentration on the rising limb of the hydrograph and a sharp decline in sediment concentration immediately before the peak water flowrate (middle panel Fig. 9). The hysteresis pattern is a clockwise loop, and this is the most commonly occurring hysteresis pattern for relatively undisturbed surface streams (Hamshaw et al., 2018). The surface streams sink to the karst aquifer and carry the sediment-laden water. Sediment pulses are attenuated and extended over longer time durations in the karst aquifer. This attenuation and longer duration is seen in Fig. 4 when comparing surface stream and spring hydrographs and sedigraphs. The attenuation and longer duration occurs because the inflow of water exceeds the outflow of water during the event, the sediment-laden water mixes with clear cave water, and the hydraulic conveyance of the aquifer is reduced relative to the surface streams. The pre-event water storage of the aquifer controls the timing of the water and sediment arrival at the spring, and therefore controls the hysteresis patterns.

The second mode of sediment transport is external sediment transport with counter-clockwise hysteresis at the spring (middle panel in Fig. 9), and this mode is attributed to the karst aquifer that is partially full of water initially. The aquifer contains unsaturated and saturated matrices. Sediment-laden water enters the aquifer, where it pushes a pulse of prior-stored clear water out of the aquifer. At the same time, the hydraulic head of the aquifer increases relatively quickly due to partial water storage causing an increased water flowrate and a peak in the hydrograph. The delay of sediment-laden water reaching the spring causes a lag in the peak of the sedigraph beyond that of the hydrograph, and in turn produces a counter-clockwise hysteresis loop.

The third mode of sediment transport in the karst cave is external sediment transport with clockwise hysteresis (bottom panel in Fig. 9). This mode is attributed to a karst aquifer that is initially very unsaturated. An initially unsaturated aquifer causes the sediment concentration peak occur early in the event before the hydrograph peak in time. The hydrograph peak does not arrive until the aquifer has become fully saturated to produce a maximum pressure response at the spring. So, the sediment reaches the spring before the aquifer is fully saturated. Clearwater is pushed out of the cave, sediment-laden water is transported through the cave to the spring, then the aquifer reaches saturation and Q peak arrives at the spring. In turn, the onset of the sediment peak arriving prior to the water flowrate peak causes the clockwise hysteresis loop (Fig. 9).

The sediment transport behavior of Fig. 9 is conceptualized for the karst system of the present study and those karst systems that show similar geomorphology. In this study, the cave draining the aquifer is always phreatic, meaning that the conduit is always filled with water. However the overlaying epigenetic aquifer has varying levels of saturation, where if the aquifer is fully saturated, then the fracture network and rock matrix is filled with water; or if it is unsaturated, where the fracture network and is not filled with water, it is at a lower potentiometric surface. The primary cave draining the aquifer is phreatic because there is a downstream control on the cave (Husic et al., 2017a,b; Al Aamery et al., 2021). Phreatic conduits are very common in the karst literature, and examples of phreatic cave studies are studied in White (2002), Drysdale et al. (2001), Massei et al. (2003), and Herman et al. (2008). If the cave is not phreatic, it is plausible that we have a behavior similar to the surface, including the first flush phenomenon, picking up sediment on the rising limb of the hydrograph, and therefore causing a clockwise hysteresis looping direction. In this case, we might expected the same commonly occuring clockwise hysteresis as surface streams. For the phreatic system as in this study, we show that the answer could be either clockwise or counterclockwise, and it is really a function of the saturation in the aquifer.

4.2. Sediment hysteresis in karst

We provide comparison of our conceptual model for Royal Spring (Fig. 9) with a meta-analysis for existing datasets from karst springs without already existing *TSS-Q* hysteresis analysis (Table 1). The studies listed in the meta-analysis were studies that provided TSS or turbidity data as well as water flowrate data for karst springs, however hysteresis loops were not carried out in these studies, and therefore we carried out the hysteresis analyses for comparison. Sediment concentration or turbidity and water flowrate data were extracted from published datasets for karst springs from Germany, Italy, France, United States, Switzerland, and Romania (Schiperski et al. 2015, Drysdale et al. 2001, Fournier et al. 2006, Reed et al. 2010, Luhmann et al. 2012, Goldscheider et al. 2010, Herman et al. 2008, Florea et al. 2019, Mahler & Lynch 1999), and hysteresis patterns were quantified using the data distributions (see our hysteresis analyses of these datasets in Fig. S3). Results are reported in Table 1, and the meta-analysis results were that 7 out of 13 results showed counterclockwise hysteresis patterns and 4 out of 13 results show clockwise hysteresis patterns. The two events from the Karst Swiss Plateau, Switzerland showed multiple patterns and loops, and investigation of this dataset and the text in the paper showed that the first half of the events showed no hysteresis associated with internal sediment followed by some looping later in the event associated with an externally originating sediment source (Goldscheider et al., 2010).

The meta-analysis results agree well with Royal Spring, and suggest commonality of counter-clockwise hysteresis with high variability resulting from pre-event water storage in the aquifers. We qualify the small number of storm events in the meta-analysis, and many papers only presented one storm event of sediment concentration or turbidity data. Nevertheless, 54 % of the meta-analysis results and 57 % of Royal Spring results (29 events) show counter-clockwise hysteresis. Applying the concept models hypothesized in Fig. 9, the meta-analysis suggests externally-sourced sediment entering karst aquifers that are partially full of water controls the commonly occurring sediment transport behavior for karst aquifers. At the same time, the presumed importance of pre-event water storage in the aquifers is reasonable with 31 % and 15 % of events showing clockwise and irregular behavior, respectively. This compares well with the overall temporal variability of Royal Spring with 44 % of events showing no hysteresis, clockwise patterns, or irregularity.

Our findings suggest an expanded view of sediment hysteresis for the *TSS-Q* patterns for phreatic karst systems beyond that of proximal and distal sediment source initiation common to surface stream interpretation (e.g., Juez et al., 2018). Results herein provide evidence that *TSS-Q* hysteresis patterns of clockwise and counter-clockwise behavior in phreatic karst reflect the pre-event water storage in the aquifer. The external sediment source and its time of initiation can be the same and the hysteresis pattern in the karst system is rather a phenomenon of antecedent water conditions.

Regarding *EC-TSS* hysteresis, results suggest that clockwise patterns occur as a result of the time-varying nature of sediment concentration entering the karst aquifer from sinking streams. This interpretation contradicts interpretation of hysteresis patterns adopted in some previous karst studies where researchers suggest resuspension of internal cave sediment causes hysteresis (Fournier et al., 2006; Schiperski et al., 2015; Valdes et al., 2006). Fournier et al. (2006) states that clockwise hysteresis for *EC-TSS* is due to resuspension of previously deposited sediment and counter-clockwise hysteresis for *EC-TSS* is due to deposition of sediment onto the cave floor. This interpretation is not consistent with the mechanics of phreatic caves similar to the Royal Spring system because sediment transport occurs via fluvial erosion. One scenario where the interpretation of Fournier et al. (2006) seems reasonable could be an extensive network of dry cave bottoms with very loose, unconsolidated sediment that is resuspended as water makes contact with the sediment. This phenomenon will be similar to a first flush in surface dominated watersheds. However, for phreatic caves that already have sinking streams flowing through them, we see no available sediment mechanics to suggest a first flush phenomenon.

Table 1
Meta-analysis results.

Karst Spring and Location	Q range	TSS or turbidity range	Hysteresis result (see also Supplemental Fig. S1)	Journal Paper
a) Gallusquelle Karst Spring, Germany	N/A	1 NTU–115 NTU	Counter-Clockwise or Inconclusive	Schiperski et al., 2015
b) Cartaro Springs, Italy	N/A	0 mg/L–2000 mg/L	Counter-clockwise	Drysdale et al., 2001
c) Pays de Coux Hannetot Spring, France	16 cms–75 cms	0 NTU–575 NTU	Clockwise	Fournier et al., 2007
d) Blue Hole Spring, Kentucky, United States	0.025 cms–3.4 cms	5–93.8 NTU 30 mg/L–654 mg/L	Clockwise	Reed et al., 2010
e) SP-2, Kentucky, United States	0.012 cms–1.65 cms	4.5 NTU–308 NTU 300 mg/L–803 mg/L	Counter-Clockwise	Reed et al., 2010
f) Freiheit Spring, Minnesota, United States	0.025 cms–0.0358 cms (25 L/s–35.8 L/s)	0 mg/L–2.1 × 10^{-3} mg/L (0 g sediment/ g water–2.1 × 10^{-3} g sediment/g water)	Counter-Clockwise	Luhmann et al., 2012
g) Karst Swiss Plateau–Moulinet Spring, Switzerland	0.02 cms–0.210 cms (20 L/s–210 L/s)	0 NTU–8 NTU	Multiple loops	Goldscheider et al., 2010
h) Karst Swiss Plateau–Moulinet Spring, Switzerland	0.025 cms–0.13 cms (25 L/s–130 L/s)	0 NTU–3.2 NTU	Irregular	Goldscheider et al., 2010
i) Arch Spring, Pennsylvania, United States	2 cms–375 cms	95 mg/L–940 mg/L	Clockwise	Herman et al., 2008
j) Vadu Crisului Karst Basin, Romania	0.111 cms–1.111 cms (1.0 × 10^5 L/ 15-min–1.0 × 10^6 L/15-min)	0 NTU–27.5 NTU	Counter-Clockwise	Florea et al., 2019
k) Vadu Crisului Karst Basin, Romania	0.222 cms–0.667 cms (2.0 × 10^5 L/ 15-min–6.0 × 10^5 L/15-min)	0 NTU–5 NTU	Counter-Clockwise	Florea et al., 2019
l) Barton Springs, Texas, United States	1.5 cms–1.95 cms	1 mg/L–13 mg/L	Clockwise	Mahler and Lynch, 1999
m) Barton Springs, Texas, United States	0.7 cms–1.25 cms	3 mg/L–20 mg/L	Counter-Clockwise	Mahler and Lynch, 1999

5. Conclusion

Sediment transport investigation in the karst aquifer suggests potential controls on internal versus external sediment origin and the impact of aquifer saturation on hysteresis. Twenty percent of events measured at Royal Spring were characterized by transport of internal cave sediment only, which is associated with fully saturated aquifer conditions prior to the event that causes limited external inputs, is proportional to fluid shear in the subsurface cave, and can be modeled by a modified formulation of the Partheniades equation. The remaining 80 % of events were characterized to include both externally-originated and internally-resuspended sediment. Transport of externally-sourced sediment caused pulses of sediment through the karst aquifer and prolongs the duration of sediment discharge at the spring. The arrival time of sediment pulses is predictable using a metric of the amount of pre-event water storage. The pre-event water storage, or aquifer saturation, is also suggested to control sediment hysteresis results. Hysteresis shows a shift from clockwise patterns for the sinking streams to highly-variably, counter-clockwise patterns for the karst spring. Results suggest that sediment hysteresis at the spring is a function of pre-event water storage, contrasting interpretations for surface systems that state sediment hysteresis depends on the distribution of proximal to distal sediment sources. meta-analysis of ten karst springs shows counter-clockwise patterns are the most common result found for sediment hysteresis. Review of the literature suggests that clockwise patterns are more common for surface stream systems, whereas the opposite may be true for karst's underground stream systems. This difference may be a function of pre-event water storage in karst, which alters flow pathway connectivity in a way that is not possible in purely surface systems.

CRediT authorship contribution statement

Leonie Bettel: Data curation, Formal analysis, Investigation, Methodology, Software, Validation, Visualization, Writing – original draft, Writing – review & editing. **Jimmy Fox:** Conceptualization, Data curation, Funding acquisition, Investigation, Methodology, Project administration, Resources, Supervision, Writing – original draft, Writing – review & editing. **Admin Husic:** Conceptualization, Formal analysis, Methodology, Visualization, Writing – review & editing. **Junfeng Zhu:** Funding acquisition, Project administration, Resources, Supervision, Writing – review & editing. **Nabil Al Aamery:** Investigation, Methodology, Writing – review & editing. **Tyler Mahoney:** Conceptualization, Data curation, Methodology, Writing – review & editing. **Ariel Gold-McCoy:** Data curation, Writing – review & editing.

Declaration of Competing Interest

The authors declare that they have no known competing financial interests or personal relationships that could have appeared to influence the work reported in this paper.

Data availability

Data will be made available on request.

Acknowledgements

We gratefully acknowledge the financial support of this research from the Kentucky Senate Bill 271B Water Quality program and National Science Foundation Awards #1632888 and #1933779.

Appendix A. Supplementary data

Supplementary data to this article can be found online at https://doi.org/10.1016/j.jhydrol.2022.128391.

References

Al Aamery, N., Adams, E., Fox, J., Husic, A., Zhu, J., Gerlitz, M., Agouridis, C., Bettel, L., 2021. Numerical model development for investigating hydrologic pathways in shallow fluviokarst. J. Hydrol. 593, 125844 https://doi.org/10.1016/j.jhydrol.2020.125844.

Bettel, L. (2021). Sediment transport investigation in a karst basin defines governing transport processes and explains hysteresis patterns [Master's Thesis]. https://uknowledge.uky.edu/ce_etds/114/.

Cao, L., Liu, S., Wang, S., Cheng, Q., Fryar, A.E., Zhang, L., Zhang, Z., Yue, F., Peng, T., 2021. Factors controlling discharge-suspended sediment hysteresis in karst basins, southwest China: Implications for sediment management. J. Hydrol. 594, 125792 https://doi.org/10.1016/j.jhydrol.2020.125792.

Cheng, Q., Wang, S., Peng, T., Cao, L., Zhang, X., Buckerfield, S.J., Zhang, Y., Collins, A. L., 2020. Sediment sources, soil loss rates and sediment yields in a Karst plateau catchment in Southwest China. Agric. Ecosyst. Environ. 304, 107114 https://doi.org/10.1016/j.agee.2020.107114.

Clare, E. (2019). Decomposing a watershed's nitrate signal using spatial sampling and continuous sensor data [Master's Thesis]. https://uknowledge.uky.edu/ce_etds/87.

Currens, J. C., Taylor, C. J., Webb, S., Zhu, J., Workman, S., Agouridis, C., Fox, J., & Husic, A. (2015). Initial Findings from the Karst Water Instrumentation System Station, Royal Spring Groundwater Basin, Kentucky Horse Park 2010-2014. *Proceedings Kentucky Water Resources Annual Symposium, Kentucky Water Resources Research Institute*. Lexington, Kentucky, p. 9-10.

Dahaan, S.A.M.A., Al-Ansari, N., Knutsson, S., 2016. Influence of Groundwater Hypothetical Salts on Electrical Conductivity Total Dissolved Solids. Engineering 08 (11), 823–830. https://doi.org/10.4236/eng.2016.811074.

Dogwiler, T., Wicks, C.M., 2004. Sediment entrainment and transport in fluviokarst systems. J. Hydrol. 295 (1–4), 163–172. https://doi.org/10.1016/j.jhydrol.2004.03.002.

Drysdale, R., Pierotti, L., Piccini, L., Baldacci, F., 2001. Suspended sediments in karst spring waters near Massa (Tuscany), Italy. Environ. Geol. 40 (8), 1037–1050. https://doi.org/10.1007/s002540100311.

Eder, A., Strauss, P., Krueger, T., Quinton, J.N., 2010. Comparative calculation of suspended sediment loads with respect to hysteresis effects (in the Petzenkirchen catchment, Austria). J. Hydrol. 389 (1), 168–176. https://doi.org/10.1016/j.jhydrol.2010.05.043.

Eludoyin, A.O., Griffith, B., Orr, R.J., Bol, R., Quine, T.A., Brazier, R.E., 2017. An evaluation of the hysteresis in chemical concentration–discharge (C–Q) relationships from drained, intensively managed grasslands in southwest England. Hydrol. Sci. J. 62 (8), 1243–1254. https://doi.org/10.1080/02626667.2017.1313979.

Florea, L.J., Banks, S.M., Forray, F.L., 2019. Importance of suspended sediments and dissolved organic carbon to carbon exports in karst – The Vadu Crişului karst basin in the Pădurea Craiului Mountains, Romania. Chem. Geol. 527, 118735 https://doi.org/10.1016/j.chemgeo.2018.04.015.

Fournier, M., Massei, N., Bakalowicz, M., Dussart-Baptista, L., Rodet, J., Dupont, J.P., 2006. Using turbidity dynamics and geochemical variability as a tool for understanding the behavior and vulnerability of a karst aquifer. Hydrogeol. J. 15 (4), 689–704. https://doi.org/10.1007/s10040-006-0116-2.

Fournier, M., Massei, N., Bakalowicz, M., Dussart-Baptista, L., Rodet, J., Dupont, J.P., 2007. Using turbidity dynamics and geochemical variability as a tool for understanding the behavior and vulnerability of a karst aquifer. Hydrogeol J. 15, 689–704. https://doi.org/10.1007/s10040-006-0116-2.

Fraley, D., 2019. About Us - Georgetown Municipal Water and Sewer Service. Gmwss.com. https://gmwss.com/about.htm.

Georgia Coastal Ecosystems LTER. (n.d.). *GCE Data Toolbox for MATLAB*. https://gce-lter.marsci.uga.edu/gce_toolbox/.

Goldscheider, N., Pronk, M., Zopfi, J., 2010. New insights into the transport of sediments and microorganisms in karst groundwater by continuous monitoring of particle-size distribution. Geologia Croatica 63 (2). https://doi.org/10.4154/gc.2010.10.

Hamshaw, S.D., Dewoolkar, M.M., Schroth, A.W., Wemple, B.C., Rizzo, D.M., 2018. A New Machine-Learning Approach for Classifying Hysteresis in Suspended-Sediment Discharge Relationships Using High-Frequency Monitoring Data. Water Resour. Res. 54 (6), 4040–4058. https://doi.org/10.1029/2017wr022238.

Hanson, G.J., Simon, A., 2001. Erodibility of cohesive streambeds in the loess area of the midwestern USA. Hydrol. Process. 15 (1), 23–38. https://doi.org/10.1002/hyp.149.

Hartmann, A., Mudarra, M., Andreo, B., Marín, A., Wagener, T., Lange, J., 2014. Modeling spatiotemporal impacts of hydroclimatic extremes on groundwater recharge at a Mediterranean karst aquifer. Water Resour. Res. 50 (8), 6507–6521. https://doi.org/10.1002/2014wr015685.

Heathwaite, A.L., Bieroza, M., 2020. Fingerprinting hydrological and biogeochemical drivers of freshwater quality. Hydrol. Process. 35 (1) https://doi.org/10.1002/hyp.13973.

Herman, E.K., Toran, L., White, W.B., 2008. Threshold events in spring discharge: Evidence from sediment and continuous water level measurement. J. Hydrol. 351 (1–2), 98–106. https://doi.org/10.1016/j.jhydrol.2007.12.001.

Husic, A., Fox, J., Agouridis, C., Currens, J., Ford, W., Taylor, C., 2017a. Sediment carbon fate in phreatic karst (Part 1): Conceptual model development. J. Hydrol. 549, 179–193. https://doi.org/10.1016/j.jhydrol.2017.03.052.

Husic, A., Fox, J., Ford, W., Agouridis, C., Currens, J., Taylor, C., 2017b. Sediment carbon fate in phreatic karst (Part 2): Numerical model development and application. J. Hydrol. 549, 208–219. https://doi.org/10.1016/j.jhydrol.2017.03.059.

Husic, A., Fox, J., Adams, E., Backus, J., Pollock, E., Ford, W., Agouridis, C., 2019. Inland impacts of atmospheric river and tropical cyclone extremes on nitrate transport and stable isotope measurements. Environ. Earth Sci. 78 (1) https://doi.org/10.1007/s12665-018-8018-x.

Husic, A. (2015). Sediment organic carbon fate and transport in a fluviokarst watershed in the Bluegrass Region [Master's Thesis]. https://uknowledge.uky.edu/ce_etds/30.

Juez, C., Hassan, M.A., Franca, M.J., 2018. The origin of fine sediment determines the observations of suspended sediment fluxes under unsteady flow conditions. Water Resour. Res. 54, 5654–5669. https://doi.org/10.1029/2018WR022982.

Juez, C., Garijo, N., Hassan, M.A., Nadal-Romero, E., 2021. Intraseasonal-to-Interannual Analysis of Discharge and Suspended Sediment Concentration Time-Series of the Upper Changjiang (Yangtze River). Water Resour. Res. 57 (8) https://doi.org/10.1029/2020wr029457.

Krajewski, A., Gładecki, J., Banasik, K., 2018. Transportation of sediment carried during flood events in a small urban catchment. Acta Scientiarum Polonorum Formatio Circumiectus 3, 119–127. https://doi.org/10.15576/asp.fc/2018.17.3.119.

Lefrançois, J., Grimaldi, C., Gascuel-Odoux, C., Gilliet, N., 2007. Suspended sediment and discharge relationships to identify bank degradation as a main sediment source on small agricultural catchments. Hydrol. Process. 21 (21), 2923–2933. https://doi.org/10.1002/hyp.6509.

Leibundgut, C. (1998). Vulnerability of karst aquifers (pp. 45–60). Karst Hydrology (Proceedings of Workshop W2 held at Rabat, Morocco, April-May 1997).

Liu, W., Birgand, F., Tian, S., Chen, C., 2021. Event-scale hysteresis metrics to reveal processes and mechanisms controlling constituent export from watersheds: A review☆. Water Res. 200, 117254 https://doi.org/10.1016/j.watres.2021.117254.

Lloyd, C.E.M., Freer, J.E., Johnes, P.J., Collins, A.L., 2016. Using hysteresis analysis of high-resolution water quality monitoring data, including uncertainty, to infer controls on nutrient and sediment transfer in catchments. Sci. Total Environ. 543, 388–404. https://doi.org/10.1016/j.scitotenv.2015.11.028.

Luhmann, A.J., Covington, M.D., Alexander, S.C., Chai, S.Y., Schwartz, B.F., Groten, J.T., Alexander, E.C., 2012. Comparing conservative and nonconservative tracers in karst and using them to estimate flow path geometry. J. Hydrol. 448–449, 201–211. https://doi.org/10.1016/j.jhydrol.2012.04.044.

Mahler, B.J., Lynch, F.L., 1999. Muddy waters: temporal variation in sediment discharging from a karst spring. J. Hydrol. 214 (1–4), 165–178. https://doi.org/10.1016/s0022-1694(98)00287-x.

Massei, N., Wang, H.Q., Dupont, J.P., Rodet, J., Laignel, B., 2003. Assessment of direct transfer and resuspension of particles during turbid floods at a karstic spring. J. Hydrol. 275 (1–2), 109–121. https://doi.org/10.1016/s0022-1694(03)00020-9.

Nerantzaki, S.D., Giannakis, G.V., Efstathiou, D., Nikolaidis, N.P., Sibetheros, I.A., Karatzas, G.P., Zacharias, I., 2015. Modeling suspended sediment transport and assessing the impacts of climate change in a karstic Mediterranean watershed. Sci. Total Environ. 538, 288–297. https://doi.org/10.1016/j.scitotenv.2015.07.092.

Paylor, R., Currens, J., 2004. Royal spring karst groundwater travel time investigation. A report prepared for Georgetown Municipal Water and Sewer Service, Lexington, KY.

Pellerin, B.A., Wollheim, W.M., Feng, X., Vörösmarty, C.J., 2008. The application of electrical conductivity as a tracer for hydrograph separation in urban catchments. Hydrol. Process. 22 (12), 1810–1818. https://doi.org/10.1002/hyp.6786.

Reed, T.M., Todd McFarland, J., Fryar, A.E., Fogle, A.W., Taraba, J.L., 2010. Sediment discharges during storm flow from proximal urban and rural karst springs, central Kentucky, USA. J. Hydrol. 383 (3–4), 280–290. https://doi.org/10.1016/j.jhydrol.2009.12.043.

Schiperski, F., Zirlewagen, J., Hillebrand, O., Nödler, K., Licha, T., Scheytt, T., 2015. Relationship between organic micropollutants and hydro-sedimentary processes at a karst spring in south-west Germany. Sci. Total Environ. 532, 360–367. https://doi.org/10.1016/j.scitotenv.2015.06.007.

Spangler, L. E. (1982). Karst hydrogeology of northern Fayette and southern Scott counties, Kentucky.

Taylor, C. J. (1992). Ground-water occurrence and movement associated with sinkhole alignments in the Inner Bluegrass Karst Region of central Kentucky.

Thrailkill, J., & Gouzie, D. R. (1984). Discharge and travel time determinations in the Royal Spring groundwater basin, Kentucky.

Tripathi, G. N. (2009). Use of surface geophysical techniques to locate a karst conduit in the cane run-royal spring basin, kentucky.

United States Environmental Protection Agency (USEPA). (1999). *Standard operating procedure for the analysis of residue, nonfilterable (suspended solids), water, method 160.2 NS (Gravimetric, 103-105oC)*.

Valdes, D., Dupont, J.-P., Massei, N., Laignel, B., Rodet, J., 2006. Investigation of karst hydrodynamics and organization using autocorrelations and T-ΔC curves. J. Hydrol. 329 (3–4), 432–443. https://doi.org/10.1016/j.jhydrol.2006.02.030.

Walling, D.E., Collins, A.L., Jones, P.A., Leeks, G.J.L., Old, G., 2006. Establishing fine-grained sediment budgets for the Pang and Lambourn LOCAR catchments. UK. *Journal of Hydrology* 330 (1–2), 126–141. https://doi.org/10.1016/j.jhydrol.2006.04.015.

White, W.B., 2002. Karst hydrology: recent developments and open questions. Eng. Geol. 65 (2–3), 85–105. https://doi.org/10.1016/s0013-7952(01)00116-8.

Williams, G.P., 1989. Sediment concentration versus water discharge during single hydrologic events in rivers. J. Hydrol. 111 (1–4), 89–106. https://doi.org/10.1016/0022-1694(89)90254-0.

Zarnaghsh, A., Husic, A., 2021. Degree of Anthropogenic Land Disturbance Controls Fluvial Sediment Hysteresis. Environ. Sci. Technol. 55 (20), 13737–13748. https://doi.org/10.1021/acs.est.1c00740.